Title

Near-atomic cryo-EM imaging of a small protein displayed on a designed scaffolding system

Journal

Proceedings of the National Academy of Sciences of the United States of America, 115(13)

ISSN

0027-8424

Authors

Liu, Yuxi
Gonen, Shane
Gonen, Tamir
et al.

Publication Date

2018-03-27

DOI

10.1073/pnas.1718825115

Peer reviewed

Near-atomic cryo-EM imaging of a small protein displayed on a designed scaffolding system

Yuxi Liu[a,1], Shane Gonen[b,c,1], Tamir Gonen[d,e], and Todd O. Yeates[a,f,g,2]

[a]Department of Chemistry and Biochemistry, University of California, Los Angeles, CA 90095; [b]Howard Hughes Medical Institute, Janelia Research Campus, Ashburn, VA 20147; [c]Howard Hughes Medical Institute, University of California, San Francisco, CA 94143; [d]Howard Hughes Medical Institute, Department of Physiology, David Geffen School of Medicine, University of California, Los Angeles, CA 90095; [e]Howard Hughes Medical Institute, Department of Biological Chemistry, David Geffen School of Medicine, University of California, Los Angeles, CA 90095; [f]UCLA-DOE Institute for Genomics and Proteomics, Los Angeles, CA 90095; and [g]UCLA Molecular Biology Institute, Los Angeles, CA 90095

Edited by Robert M. Stroud, University of California, San Francisco, California, and approved February 5, 2018 (received for review October 27, 2017)

Current single-particle cryo-electron microscopy (cryo-EM) techniques can produce images of large protein assemblies and macromolecular complexes at atomic level detail without the need for crystal growth. However, proteins of smaller size, typical of those found throughout the cell, are not presently amenable to detailed structural elucidation by cryo-EM. Here we use protein design to create a modular, symmetrical scaffolding system to make protein molecules of typical size suitable for cryo-EM. Using a rigid continuous alpha helical linker, we connect a small 17-kDa protein (DARPin) to a protein subunit that was designed to self-assemble into a cage with cubic symmetry. We show that the resulting construct is amenable to structural analysis by single-particle cryo-EM, allowing us to identify and solve the structure of the attached small protein at near-atomic detail, ranging from 3.5- to 5-Å resolution. The result demonstrates that proteins considerably smaller than the theoretical limit of 50 kDa for cryo-EM can be visualized clearly when arrayed in a rigid fashion on a symmetric designed protein scaffold. Furthermore, because the amino acid sequence of a DARPin can be chosen to confer tight binding to various other protein or nucleic acid molecules, the system provides a future route for imaging diverse macromolecules, potentially broadening the application of cryo-EM to proteins of typical size in the cell.

cryo-electron microscopy | protein design | DARPin | protein cage | protein scaffold

Recent advancements have brought single-particle electron microscopy (EM) techniques to the forefront of structural biology (1–3). In favorable cases, 3D cryo-EM image reconstruction methods can produce structures of macromolecular complexes at atomic level detail (4–9). In such studies, very large macromolecular assemblies offer important advantages in signal processing and imaging, and this advantage is enhanced in systems that are highly symmetric—e.g., composed of numerous repeating copies of one or a few protein building blocks. For those reasons, viral capsids are quintessential examples for favorable cryo-EM reconstruction. At the other end of the spectrum, however, individual protein molecules of typical size (e.g., 50 kDa or smaller), which lack the aforementioned advantages, remain extremely difficult to visualize at atomic detail by EM. This critical size limitation represents a singular impediment to the universal application of EM for elucidating the structures of most proteins in the human genome.

Recent studies have shown that small proteins can be computationally redesigned so that multiple copies of the protein subunit will self-assemble into large, symmetric cages with shapes resembling regular geometric solids, e.g., a tetrahedron, cube, or icosahedron (10–16). The structures resulting from some of these designed assembly approaches have sufficiently large mass and high symmetry to allow ready analysis by cryo-EM. However, current methods for designing protein assemblies are laborious and unpredictable, often requiring substantial trial-and-error experiments and previous structural knowledge to achieve success. Those challenges have made it impractical to take a given target protein of interest, whose structure might not be known, and engineer it to assemble into a large symmetric assembly that would be amenable to cryo-EM.

It would advance cryo-EM applications tremendously if it were possible to easily attach a protein of interest to a symmetric scaffold in a rigid way, so that many copies of the target protein would be displayed in well-defined, symmetric orientations. Being able to turn a given protein into its own kind of capsid structure would give it the features of large size and symmetry that are critically advantageous for cryo-EM imaging. In the present study, we explored a route toward achieving that goal (Fig. 1*A*).

Results

To design a modular cryo-EM scaffold, we took as a starting point a set of protein cages designed by King et al. (14), specifically those built from 24 subunits, four trimers of two different subunit types. These assemble with the different trimer types sitting at alternating corners of a cube, in arrangements that obey tetrahedral symmetry. In this study, we focused our attention on designed protein cages in which one or both component subunit types contain at least one alpha helical terminus. Through further design, we extended the alpha helical terminus of the cage protein by genetic fusion to join the alpha helical terminus of a small protein target of only ~17 kDa known as

Significance

New electron microscopy (EM) methods are making it possible to view the structures of large proteins and nucleic acid complexes at atomic detail, but the methods are difficult to apply to molecules smaller than approximately 50 kDa, which is larger than the size of the average protein in the cell. The present work demonstrates that a protein much smaller than that limit can be successfully visualized when it is attached to a large protein scaffold designed to hold 12 copies of the attached protein in symmetric and rigidly defined orientations. The small protein chosen for attachment and visualization can be modified to bind to other diverse proteins, opening a new avenue for imaging cellular proteins by cryo-EM.

Author contributions: Y.L., T.G., and T.O.Y. designed research; Y.L. and S.G. performed research; Y.L., S.G., T.G., and T.O.Y. analyzed data; and Y.L., S.G., T.G., and T.O.Y. wrote the paper.

The authors declare no conflict of interest.

This article is a PNAS Direct Submission.

Data deposition: The atomic coordinates and structure factors have been deposited in the Protein Data Bank, www.wwpdb.org (PDB ID codes 6C9I and 6C9K) and to the EM Data Bank (EMDB codes EMD-7403, EMD-7436, and EMD-7437).

[1]Y.L. and S.G. contributed equally to this work.

[2]To whom correspondence should be addressed. Email: yeates@mbi.ucla.edu.

This article contains supporting information online at www.pnas.org/lookup/suppl/doi:10.1073/pnas.1718825115/-/DCSupplemental.

Published online March 5, 2018.

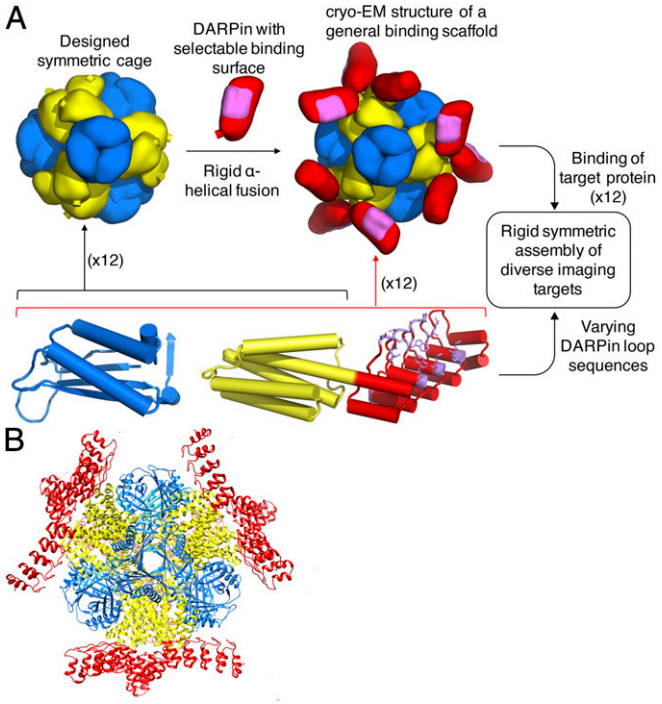

Fig. 1. A molecular scaffolding system for modular display of macromolecules for cryo-EM imaging. (*A*) Schematic diagram for a scaffolding system built on a designed symmetric protein cage. The example shown is a tetrahedrally symmetric cage with 24 subunits in $a_{12}b_{12}$ stoichiometry (A subunits in yellow and B subunits in blue). At least one of the subunits needs to have an α-helical terminus (cylinder). The α-helical termini of the cage subunit (yellow) and the DARPin subunit (red) can be joined in a rigid fashion through genetic fusion, forming a general binding scaffold. The cryo-EM structure of a binding scaffold is solved in this study. The DARPin subunit contains variable loops (highlighted in pink) whose amino acid sequence can be selected to confer binding to a wide range of specific macromolecules of interest. In principle, binding a macromolecule of interest to the designed scaffold results in the symmetric display of 12 copies of the molecule. (*B*) Detailed view of the specific scaffold, DARP14, that was designed and characterized in this study, with subunits colored as in *A*.

DARPin (Designed Ankyrin Repeat Protein) (17). This design element, fusing two proteins with terminal helices, is intended to create a semirigid and geometrically predictable helical connection spanning between two proteins that would otherwise be flexibly joined (Fig. 1*A*). This idea was developed by Padilla et al. (10) and subsequently expanded on and validated in various contexts, including various DARPin designs (11, 18–22).

The choice of a DARPin as the first fusion partner to the cage is critical, as DARPins have been developed as a general platform for binding other protein molecules. Through genetic selection techniques, amino acid sequence changes in loop regions of the DARPin protein can be identified for conferring tight binding to various target proteins of interest (23–26). In addition, their largely alpha helical nature makes DARPins suitable for fusion to other proteins by the continuous alpha helical fusion approach. The essence of our scaffolding system is that a rigid protein cage forming a core structure presents (as genetic fusions) 12 rigid and symmetrically disposed DARPin proteins projecting outward (Fig. 1). In the future, loop sequences specific for binding some other target protein can be readily exchanged into the basic DARPin structure, thereby enabling the facile capsid-like assembly of varied target proteins. Importantly, this strategy ultimately circumvents the need to perform engineering experiments on future targets themselves by restricting design efforts to the protein cage and its fused DARPin.

We experimentally tested several variations in the amino acid sequence and length of the helical connection between the cage subunit and the DARPin based on computationally generated fusion models (*Methods* and *Supporting Information*). We devoted our efforts to specific design choices that disposed the DARPin binding surfaces in highly accessible orientations for subsequent utility in binding cognate target proteins. Among the designs investigated, five could be purified in soluble form from a bacterial overexpression system and were shown to self-assemble into structures of the expected size and shape by negative stain EM (Fig. S1).

We next pursued a full structural elucidation for one of the scaffold designs, referred to here as DARP14, by 3D cryo-EM reconstruction (Figs. 2 and 3 and Table S1). DARP14 was imaged on a Titan Krios using a K2 direct electron detector (*Methods*). A total of 3,665 movies were recorded for motion correction, and after reference-free 2D classification, 229,953 particles were selected for 3D analysis. In the raw cryo-EM images, the core of the protein cage was discernible, but the individual DARPin components appeared weaker or were practically invisible (Fig. 2*A*). This finding was expected, and further supports the well-known challenge of imaging small protein molecules on their own. Subsequent 2D class averages and 3D reconstruction showed the powerful advantage of being able to locate and apply symmetry averaging to the smaller DARPin components when displayed on the engineered scaffold (Figs. 2 and 3). A 3D analysis of the cage-core based on a subset of 34,650 particles produced a reconstruction with most of the core at an atomic resolution of ∼2.5 Å, with an overall resolution of ∼3.1 Å (Fig. 2*C*, Table S1, and Movie S1). The side chains of the amino acids in the core of the cage are clearly discernible in the resulting density maps and are consistent with the designed protein. This demonstrates the use of single particle cryo-EM for solving the atomic resolution structure of a designed protein.

Importantly, much of the attached DARPin was also visible in the 2D class images (Fig. 3*A*) and reconstructions. To account for the possibility of slight variations in the orientations of the attached DARPins, which would compromise their resolution, we applied subsequent classification and refinement, including masking out the B type subunit of the cage to focus on the DARPin component (*Methods*). This substantially improved the structural details visible for the DARPin, resulting in a ∼3.5-Å resolution structure overall (Fig. 3 *B* and *C*) and allowing us to clearly model the helical secondary structural elements within the density (Fig. 3*D*) in configurations consistent with the known crystal structure of the DARPin [Protein Data Bank (PDB) ID code 3ZU7] (Table S2 and Movie S2).

The DARPin protein that we attached to the cage comprises five repeats of a common structural motif (the ankyrin repeat). In our final 3D reconstruction of the DARPin, the first four repeats could be resolved at near-atomic detail, with the local resolution worsening from 3.5 Å to 5 Å toward the tip of the structure (Fig. 3*C*). This worsening resolution toward the tips of cryo-EM structures has been observed in other cryo-EM studies (27). Moreover, we suspect that the fifth DARPin repeat in our designed scaffold may be flexible and partially unwound, further contributing to its weakness in the final image. Consistent with this explanation, the thermal vibration parameters (B-factors) in previous crystal structures of DARPins are higher for this region of the protein (28, 29) (Fig. S2). We note that this tendency toward terminal unwinding is not an impediment to forming a well-ordered complex between a DARPin and its cognate target, as has been demonstrated in multiple previous crystal structures in which the DARPin and its target are well ordered when bound together (24, 30–32). Notwithstanding the loss of resolution at the end of the attached DARPin, this result demonstrates that the structure of a small protein can be visualized at near-atomic resolution by a cryo-EM scaffolding approach.

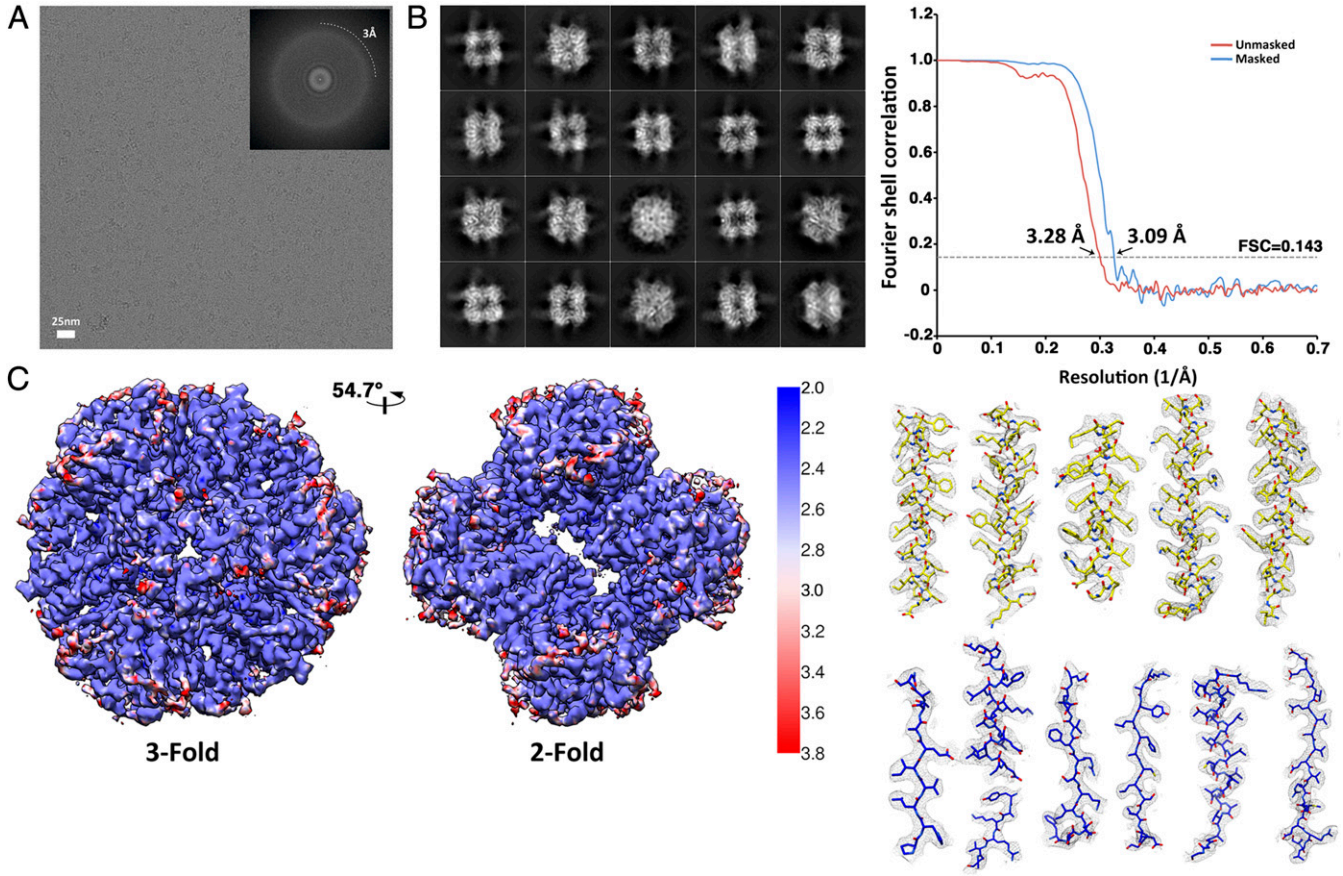

Fig. 2. Cryo-EM structure of DARP14 symmetric cage core. (*A*) Representative motion-corrected cryo-electron micrograph of DARP14. (*Inset*) Fourier transformation showing visible thon rings to ∼3 Å. (*B*) Reference-free 2D class averages highlighting good alignment of the cage and clear density for fused 17-kDa DARPins. (*C*) Overview of a ∼3.1-Å reconstruction of the cage core. (*Left*) Representations of unfiltered local resolution viewing down the threefold and twofold symmetry axes highlighting extensive areas at atomic resolutions of ∼2.5 Å. (*Top Right*) Fourier shell correlation (FSC) curves of unmasked and masked reconstructions. (*Bottom Right*) Refined model fit into density for subunit A (yellow) and subunit B (blue) of the cage core. All secondary structure elements are represented along with selected loop regions.

Discussion

Our analysis demonstrates that the alpha helical fusion scheme used here provides a connection between the symmetric cage and the DARPin that is sufficiently rigid to enable near–atomic-resolution imaging. This is a critical result, as it was not known in advance whether the alpha helical fusion would hold the DARPin in a sufficiently ordered configuration. The ordered nature of the DARPin was evident in preliminary 2D averaging (Fig. 3*A*) even before 3D reconstruction and application of symmetry to optimize the imaging of the cage. When comparing our final structure to the initial computational model, a minor reorientation of the DARPin component (by ∼13°) is evident (Fig. 3*E* and Fig. S3). Among the several designs that we explored (Fig. S1), the structure of the design analyzed here appears to be influenced, beyond our designed continuous alpha helical fusion, by a few additional atomic contacts between the DARPin and the cage subunits. These contacts likely help stabilize the DARPin in a well-defined orientation on the scaffolding cage. The relatively high orientational rigidity that we obtained for the DARPin promises good prospects for similarly rigid attachment of other proteins to the DARPin for their visualization in subsequent studies. Previous studies of DARPin complexes indicate stable and rigid binding to their cognate protein targets (21, 26–28).

Our results emphasize two major points. First, the DARPin component is a small protein (17 kDa) whose separate structure would otherwise be impossible to resolve by single particle cryo-EM methods. However, it can be visualized in near–atomic-resolution detail when its image is reconstructed in the context of rigid assembly on a large symmetric protein cage. In recent work, Coscia et al. (33) was able to image a larger (40 kDa) target protein fused to a natural protein scaffold at lower resolution (local resolution between 6 and 10 Å), and only after extensive biochemical analysis and optimization of linker lengths. We show here that a rational design of a continuous alpha helical attachment to a cubically symmetric designed protein cage can provide the rigidity required to achieve near-atomic resolutions even for a small, 17-kDa attached target protein. Since our present scaffold was the best among only a relatively small number of candidates investigated, it is likely that further design efforts could improve the degree of rigidity, making it possible to reach an even better spatial resolution. Second, our development of a DARPin as the fused protein component introduces a critical element of modularity. Building on this system, the challenging molecular engineering required to create symmetric architectures will not need to be repeated for each application to a new target protein to be imaged. In principle, no modification to a target protein is required, because the loop sequences of the DARPin carried on the scaffold can be mutated to bind various target proteins in their native forms.

The ease of attachment and rigidity of cognate target proteins bound to the scaffold are key issues for future studies. It is

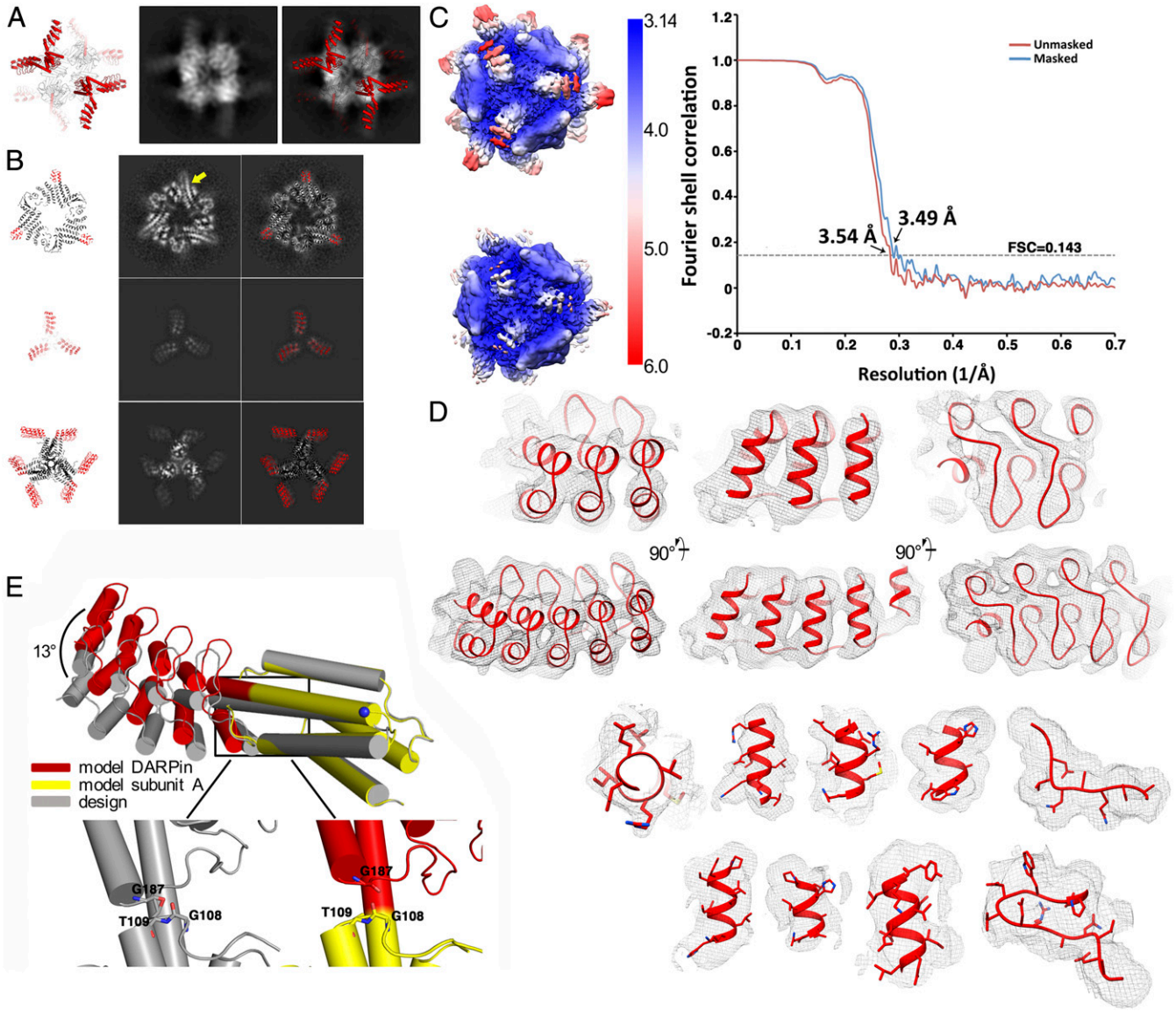

Fig. 3. Cryo-EM reconstruction of DARPin displayed on the symmetric cage. (*A*) Comparison of the DARP14 design (DARPins and their extended helix in red and cage subunits A and B in black and white, respectively) to one 2D class average, with an overlay (*Right*) highlighting the density of DARPin helices protruding from the cage. (*B*) Three comparisons of the calculated model and slices of reconstructions. (*Top*) Focus on the extended helix where DARPins are fused (yellow arrow) (from map EMD-7403). (*Middle*) Top view showing the DARPin arms and clear density for each helical repeat. (*Bottom*) Side slice. (*C*) Local resolution of an unfiltered ∼3.5-Å reconstruction where the subunit A and fused DARPin were masked during refinement for higher resolution of those areas. (*Left Top*) Low contouring level to show the entire reconstruction. (*Left Bottom*) Higher contouring level highlighting the near-atomic detail of DARPin repeats. (*Right*) FSC of unmasked and masked DARPin reconstructions. (*D*) Highlights of DARPin density in different regions with the fitted model. (*Top two rows*) High sigma level highlighting DARPin helical repeats 1–3 and lower sigma level highlighting all five helical DARPin repeats as a top view (*Left*), side view (*Middle*), and bottom view (*Right*). Views are related by 90° rotations. (*Bottom two rows*) Density fit of DARPin model from various helices (including one top view of helix 2) and two views of loop regions where the amino acid sequence for the DARPin would be varied for binding to cognate target molecules. (*E*) Comparison between the computational design for DARP14 and the cryo-EM density-fitted model, showing a small displacement of the fitted model from the design. The designed DARP14 and the cryo-EM model were aligned on their A subunits (termed chain B in PDB ID code 4NWP). (*Top*) There is a ∼13° rotation around an axis going through the view of plane at the blue dot between the design and the EM model. (*Bottom*) Zoom-in at Gly-187 in the first turn on the DARPin, which is in steric clash to Gly108 and Thr-109 from subunit A in the design (*Bottom Left*). This clash is relieved in observed model and likely contributes to the DARPin stability in its currently observed orientation (*Bottom Right*).

possible that attached proteins could exhibit higher flexibility or, in contrast, could help rigidify the DARPin. Moreover, very large target proteins could create steric challenges for full-occupancy attachment. For the scaffold explored here, the closest approach between the centers of the 12 DARPin binding surfaces is approximately 65 Å, which we expect would allow the scaffold to accommodate proteins as large as 200 kDa without collisions (Fig. S4). This is notable, given that proteins larger than this size can be imaged directly without scaffolding by cryo-EM. Thus, we expect our scaffold to be compatible with most imaging targets below the current cryo-EM size limit.

Finally, different target proteins may be more or less suitable for the symmetric scaffolding approach. Proteins that naturally self-associate are likely to be problematic, for example. Indeed, we observed that the ERK2 protein that binds to the DARPin that we used in this initial study self-associates, and as a result

the scaffold could not be maintained in solution on addition of the target protein in this case (data not shown).

Ultimately, it might prove important to develop a suite of distinct scaffolding systems using variations on the design theme developed here. Each such scaffold could provide a distinct opportunity for obtaining a high-resolution structure of a target protein irrespective of how small that target protein is, as demonstrated in this study. Further developments of this scaffolding approach should ultimately enable the facile imaging of large numbers of cellular proteins whose structures have previously been beyond the reach of cryo-EM.

Materials and Methods

Computational Alpha Helix Fusion Methods. Computational alpha helix fusion models were generated similarly as in our previous work (10, 11). As a test case for fusing to a protein cage, we used a DARPin whose sequence was selected to bind to the extracellular signal-regulated kinase 2 (ERK2) and whose structure in complex with its cognate partner is known (PDB ID code 3ZU7). In choosing a protein cage as the fusion partner, we restricted our attention to those with a protein with a terminal alpha helix at least 6-aa long and with no more than 10 unstructured amino acids beyond it. The set of protein cages that satisfied this criterion included six protein assemblies designed in previous work (11, 14, 15, 34, 35).

We next tested the feasibility of pairwise joining between the protein cage subunit and the DARPin subunit. To do so, we first aligned an ideal alpha helix to the last six helical residues on the cage subunit. We then aligned the DARPin terminal helix to the ideal alpha helix. The aligned position of the DARPin on the ideal alpha helix was slid one residue at a time. The range of sliding was from a 6-residue overlap to a 15-residue insertion relative to the helical termini of the DARPin and the cage subunit. We inspected the models at each aligned position and removed those with excessive clashes. If the fusion model had overlapping helical termini, the amino acid sequence within the overlap was chosen to maintain good native contacts within each subunit. If the fusion model required an insertion between the helical termini, ER/K-rich helix segments (19, 36) were used.

The experimentally tested models were chosen to give different DARPin orientations relative to the cage subunit while providing a large space for attachment of imaging targets. The construct with the shortest linker for each DARPin orientation was selected. In total, nine constructs were deemed suitable for experimental characterization. These were based on the single DARPin noted earlier fused to one subunit of two different two-component cages, T33-21 (14) and T33-31 (35). Based on different helical lengths for connection to the DARPin, there were three candidate fusions to cage protein T33-31 and six fusions to cage protein T33-21.

Cloning, Expression, and Purification. Constructs DARP10, DARP11, DARP12, DARP14, and DARP16 were expressed and purified under conditions similar to those used for the cage proteins alone (14), with slight modifications. We purchased *Escherichia coli* codon optimized gene fragments (Integrated DNA Technologies) and inserted the sequences encoding both cage subunit A with fused DARPin and subunit B into a pET-22b vector, separated by the intergenic region of pET-DUET. Proteins were expressed in autoinduction medium at 20 °C for 2 d.

Cells were suspended and lysed in lysis buffer (50 mM Tris pH 8.0, 250 mM NaCl, and 20 mM imidazole) supplemented with DNase, lysozyme, and protease inhibitor (Pierce; Thermo Fisher Scientific). Cleared lysate was loaded onto a HisTrap column (GE Healthcare) and eluted with a linear gradient of elution buffer (50 mM Tris pH 8.0, 250 mM NaCl, and 500 mM imidazole). Pooled and concentrated fractions were then further purified with size exclusion chromatography on a Superose 6 Increase column (GE Healthcare). Fractions corresponding to intact tetrahedral assemblies were used in further analysis.

Negative Stain EM. Freshly purified proteins at approximately 50 μg/mL were applied onto glow-discharged 200- or 300-mesh copper Formvar-supported carbon grids (Ted Pella), washed with Milli-Q water, and stained with 2% uranyl acetate or 0.75% uranyl formate. Micrographs were collected using a Tecnai T12 transmission electron microscope with a bottom-mounted TVIPS F416 4K × 4K CMOS camera at a nominal magnification of 49,000× at the specimen level.

Cryo-EM.

DARP14 grid screening. Purified, concentrated DARP14 was screened for ice thickness, stability, and particle distribution using an FEI TF20 microscope equipped with a bottom-mounted TVIPS F416, 4K × 4K CMOS camera.

DARP14 grid freezing for data collection. Superose 6 Increase column (GE Healthcare)-purified, concentrated DARP14 was diluted to ∼0.5 mg/mL using 10 mM Tris pH 8.0 and 500 mM NaCl supplemented with 1 mM of freshly prepared DTT (Acros), and 4 μL was pipetted onto carbon-coated copper grids (C-Flat, 1.2/1.3 200-mesh; Electron Microscopy Sciences). The grids were blotted and frozen in liquid ethane using a Vitrobot Mark IV system (FEI) and stored for data collection under liquid nitrogen.

Data collection. Superresolution movies were collected using a Titan Krios transmission electron microscope (FEI) equipped with a Gatan K2 Summit direct electron detector at 22,500× magnification at the specimen level, with a pixel size of 1.31 Å/pixel (0.655 Å/pixel superresolution).

Data Processing.

Cryo reconstructions. Superresolution movies of frozen DARP14 were corrected for beam-induced motion using MotionCor2 (37). Particles were picked using the XMIPP software package (38). All coordinates were imported into and all unbinned micrographs analyzed using the RELION 2 software pipeline (39). An initial model was calculated de novo using the stochastic gradient descent algorithm in RELION 2.1-beta-0 using a subset of the calculated 2D classes, and 3D classification and refinements were performed, and all final refinements used enforced T symmetry. The final refined map containing DARPins was made while masking out all B subunits. Local resolution was estimated using ResMap (40) and RELION. All masks and subsequent models were created from the reconstructions using combinations of both RELION and UCSF Chimera (41). All RELION calculations were done using different versions of RELION 2 except for the final refinements, postprocessing, and local resolution estimations (including the final Fourier shell correlation calculations), which were done using RELION version 2.1-beta-1.

Structure analysis. All reconstructions were analyzed using UCSF Chimera and Coot (42). The design model was initially fit using UCSF Chimera, followed by structure relaxation in Rosetta (43, 44) without enforced symmetry. Refined models were analyzed using UCSF Chimera, PyMOL (Schrödinger), and Coot.

ACKNOWLEDGMENTS. We thank Marianne Vo for her contribution to protein production, James Evans for preliminary assistance with the EM studies, and Johan Hattne for help with the computational cluster. This work was funded by the Biological and Environmental Research program of the Department of Energy Office of Science (Award DE-FC02-2ER63421) and by a UCLA Whitcome Fellowship (to Y.L.). The T.G. laboratory is supported by the Howard Hughes Medical Institute.

1. Nogales E (2016) The development of cryo-EM into a mainstream structural biology technique. *Nat Methods* 13:24–27.
2. Glaeser RM (2016) How good can cryo-EM become? *Nat Methods* 13:28–32.
3. Merk A, et al. (2016) Breaking cryo-EM resolution barriers to facilitate drug discovery. *Cell* 165:1698–1707.
4. Campbell MG, Veesler D, Cheng A, Potter CS, Carragher B (2015) 2.8-Å resolution reconstruction of the *Thermoplasma acidophilum* 20S proteasome using cryo-electron microscopy. *eLife* 4:e06380.
5. Gao Y, Cao E, Julius D, Cheng Y (2016) TRPV1 structures in nanodiscs reveal mechanisms of ligand and lipid action. *Nature* 534:347–351.
6. Banerjee S, et al. (2016) 2.3-Å resolution cryo-EM structure of human p97 and mechanism of allosteric inhibition. *Science* 351:871–875.
7. Zhang X, et al. (2017) An atomic structure of the human spliceosome. *Cell* 169: 918–929.e14.
8. Greber BJ, et al. (2017) The cryo-electron microscopy structure of human transcription factor IIH. *Nature* 549:414–417.
9. Hirschi M, et al. (2017) Cryo-electron microscopy structure of the lysosomal calcium-permeable channel TRPML3. *Nature* 550:411–414.
10. Padilla JE, Colovos C, Yeates TO (2001) Nanohedra: Using symmetry to design self-assembling protein cages, layers, crystals, and filaments. *Proc Natl Acad Sci USA* 98: 2217–2221.
11. Lai Y-T, Cascio D, Yeates TO (2012) Structure of a 16-nm cage designed by using protein oligomers. *Science* 336:1129.
12. Fletcher JM, et al. (2013) Self-assembling cages from coiled-coil peptide modules. *Science* 340:595–599.
13. Huard DJE, Kane KM, Tezcan FA (2013) Re-engineering protein interfaces yields copper-inducible ferritin cage assembly. *Nat Chem Biol* 9:169–176.
14. King NP, et al. (2014) Accurate design of co-assembling multi-component protein nanomaterials. *Nature* 510:103–108.
15. Bale JB, et al. (2016) Accurate design of megadalton-scale two-component icosahedral protein complexes. *Science* 353:389–394.
16. Sciore A, et al. (2016) Flexible, symmetry-directed approach to assembling protein cages. *Proc Natl Acad Sci USA* 113:8681–8686.
17. Binz HK, Stumpp MT, Forrer P, Amstutz P, Plückthun A (2003) Designing repeat proteins: Well-expressed, soluble and stable proteins from combinatorial libraries of consensus ankyrin repeat proteins. *J Mol Biol* 332:489–503.

18. Strickland D, Moffat K, Sosnick TR (2008) Light-activated DNA binding in a designed allosteric protein. *Proc Natl Acad Sci USA* 105:10709–10714.
19. Sivaramakrishnan S, Spudich JA (2011) Systematic control of protein interaction using a modular ER/K α-helix linker. *Proc Natl Acad Sci USA* 108:20467–20472.
20. Batyuk A, Wu Y, Honegger A, Heberling MM, Plückthun A (2016) DARPin-based crystallization chaperones exploit molecular geometry as a screening dimension in protein crystallography. *J Mol Biol* 428:1574–1588.
21. Schütz M, et al. (2016) Generation of fluorogen-activating designed ankyrin repeat proteins (FADAs) as versatile sensor tools. *J Mol Biol* 428:1272–1289.
22. Wu Y, et al. (2017) Rigidly connected multispecific artificial binders with adjustable geometries. *Sci Rep* 7:11217.
23. Amstutz P, et al. (2005) Intracellular kinase inhibitors selected from combinatorial libraries of designed ankyrin repeat proteins. *J Biol Chem* 280:24715–24722.
24. Veesler D, et al. (2009) Crystal structure and function of a DARPin neutralizing inhibitor of lactococcal phage TP901-1: Comparison of DARPin and camelid VHH binding mode. *J Biol Chem* 284:30718–30726.
25. Plückthun A (2015) Designed ankyrin repeat proteins (DARPins): Binding proteins for research, diagnostics, and therapy. *Annu Rev Pharmacol Toxicol* 55:489–511.
26. Sennhauser G, Grütter MG (2008) Chaperone-assisted crystallography with DARPins. *Structure* 16:1443–1453.
27. Jin P, et al. (2017) Electron cryo-microscopy structure of the mechanotransduction channel NOMPC. *Nature* 547:118–122.
28. Wetzel SK, et al. (2010) Residue-resolved stability of full-consensus ankyrin repeat proteins probed by NMR. *J Mol Biol* 402:241–258.
29. Kramer MA, Wetzel SK, Plückthun A, Mittl PRE, Grütter MG (2010) Structural determinants for improved stability of designed ankyrin repeat proteins with a redesigned C-capping module. *J Mol Biol* 404:381–391.
30. Kummer L, et al. (2012) Structural and functional analysis of phosphorylation-specific binders of the kinase ERK from designed ankyrin repeat protein libraries. *Proc Natl Acad Sci USA* 109:E2248–E2257.
31. Pecqueur L, et al. (2012) A designed ankyrin repeat protein selected to bind to tubulin caps the microtubule plus end. *Proc Natl Acad Sci USA* 109:12011–12016.
32. Seeger MA, et al. (2013) Design, construction, and characterization of a second-generation DARP in library with reduced hydrophobicity. *Protein Sci* 22:1239–1257.
33. Coscia F, et al. (2016) Fusion to a homo-oligomeric scaffold allows cryo-EM analysis of a small protein. *Sci Rep* 6:30909.
34. Lai Y-T, et al. (2014) Structure of a designed protein cage that self-assembles into a highly porous cube. *Nat Chem* 6:1065–1071.
35. Bale JB, et al. (2015) Structure of a designed tetrahedral protein assembly variant engineered to have improved soluble expression. *Protein Sci* 24:1695–1701.
36. Sivaramakrishnan S, Spink BJ, Sim AYL, Doniach S, Spudich JA (2008) Dynamic charge interactions create surprising rigidity in the ER/K α-helical protein motif. *Proc Natl Acad Sci USA* 105:13356–13361.
37. Zheng SQ, et al. (2017) MotionCor2: Anisotropic correction of beam-induced motion for improved cryo-electron microscopy. *Nat Methods* 14:331–332.
38. Sorzano CO, et al. (2004) XMIPP: A new generation of an open-source image processing package for electron microscopy. *J Struct Biol* 148:194–204.
39. Scheres SHW (2016) Processing of structurally heterogeneous cryo-EM data in RELION. *Methods Enzymol* 579:125–157.
40. Kucukelbir A, Sigworth FJ, Tagare HD (2014) Quantifying the local resolution of cryo-EM density maps. *Nat Methods* 11:63–65.
41. Pettersen EF, et al. (2004) UCSF Chimera–A visualization system for exploratory research and analysis. *J Comput Chem* 25:1605–1612.
42. Emsley P, Lohkamp B, Scott WG, Cowtan K (2010) Features and development of Coot. *Acta Crystallogr D Biol Crystallogr* 66:486–501.
43. Conway P, Tyka MD, DiMaio F, Konerding DE, Baker D (2014) Relaxation of backbone bond geometry improves protein energy landscape modeling. *Protein Sci* 23:47–55.
44. Wang RY-R, et al. (2016) Automated structure refinement of macromolecular assemblies from cryo-EM maps using Rosetta. *eLife* 5:e17219.